

RSC Advances



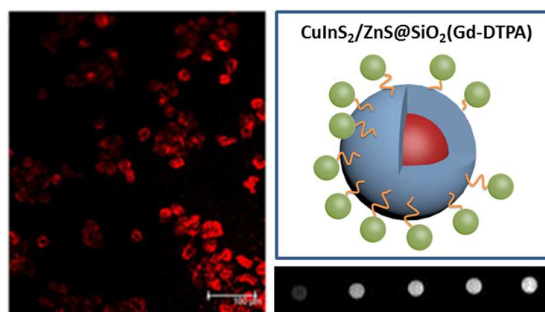
This is an *Accepted Manuscript*, which has been through the Royal Society of Chemistry peer review process and has been accepted for publication.

Accepted Manuscripts are published online shortly after acceptance, before technical editing, formatting and proof reading. Using this free service, authors can make their results available to the community, in citable form, before we publish the edited article. This *Accepted Manuscript* will be replaced by the edited, formatted and paginated article as soon as this is available.

You can find more information about *Accepted Manuscripts* in the [Information for Authors](#).

Please note that technical editing may introduce minor changes to the text and/or graphics, which may alter content. The journal's standard [Terms & Conditions](#) and the [Ethical guidelines](#) still apply. In no event shall the Royal Society of Chemistry be held responsible for any errors or omissions in this *Accepted Manuscript* or any consequences arising from the use of any information it contains.

Graphical Abstract



Multifunctional gadolinium-labeled silica-coated core/shell nanoparticles with high relaxivity and photoluminescence were synthesized as a dual-modal contrast.

Cite this: DOI: 10.1039/c0xx00000x

www.rsc.org/xxxxxx

ARTICLE TYPE

Multifunctional gadolinium-labeled silica-coated core/shell quantum dots for magnetic resonance and fluorescence imaging of cancer cells[†]

Babao Lin,^{†a} Xiuzhong Yao,^{†b} Yihua Zhu,^{a*} Jianhua Shen,^a Xiaoling Yang,^a and Chunzhong Li^a

Received (in XXX, XXX) Xth XXXXXXXXX 20XX, Accepted Xth XXXXXXXXX 20XX

DOI: 10.1039/b000000x

A new magnetic resonance (MR)/optical nanoparticles based on silica-coated CuInS₂/ZnS nanoparticles with covalent attachment of Gd³⁺ complex for cancer cells imaging is reported. We introduce silica to interdigitate with hydrophobic, protective agents on the surface of CuInS₂/ZnS nanoparticles that allows phase transfer of hydrophobic nanoparticles from the organic into aqueous phase. Carbodiimide chemistry is used to covalently couple the Gd³⁺- complex on the surface of silica-coated CuInS₂/ZnS nanoparticles for magnetic resonance and fluorescence imaging of cancer cells. The longitudinal relaxivity value is 8.45 mM⁻¹s⁻¹ for the dual-modality nanoparticles on the 3.0 T scanner, suggesting the possibility of using the nanoparticles as a T₁ contrast agent. The dual-modality nanoparticles exhibits negligible cytotoxicity with >80% cell viability in human pancreatic cancer cell lines BXPC-3 cells after 24 h. The nanoparticles with both optical and MR imaging in the aqueous solution applied to cells in culture. These results show that quantum yield and gadolinium concentration in the nanoparticles is sufficient to produce contrast for both modalities at relatively low concentrations of nanoparticles.

1. Introduction

Typical non-invasive diagnostic imaging techniques, such as fluorescence imaging, X-ray computed tomography (CT) and magnetic resonance imaging (MRI), have different sensitivities, spatial resolutions and imaging depths.¹⁻⁴ Among the various imaging technologies, MRI is one of the most powerful medical diagnosis tools because MRI can provide images with excellent anatomical details based on the soft tissue contrast and functional information in noninvasive and real-time monitoring manner.^{5,6} The sensitivity of MRI can be greatly improved by the contrast agents that enhance the contrast of the region of interest from background. The MRI contrast agents are generally categorized according to their effects on longitudinal (T₁) and transversal (T₂) relaxations, and their ability is referred to as relaxivity (r₁, r₂). The area wherein fast T₁ relaxation takes place appears bright, whereas T₂ relaxation results in the dark contrast in the MR images. T₁-weighted MR agents offer brighter contrast enhancement, which can greatly help to identify pathogenic or biological conditions of conditions of the tissues where they accumulate, and are quite frequently used in clinical disease diagnosis.^{7,8} Paramagnetic compounds with large number of unpaired electrons including Gd³⁺, Mn²⁺ are desirable for T₁ contrast because T₁ contrast effect is induced by the interactions between protons of water molecules and electron spins of the contrast agents. Gadolinium complexes, having 7 unpaired electrons in its Gd³⁺ core, are widely used as T₁ contrast agent.⁹ However, the gadolinium complexes have several disadvantages in clinical settings. The complexes generally have short circulating time due to rapid excretion through urine, which hampers the high-resolution imaging that requires long scan time.

Despite its attractive properties, sensitivity of MR imaging is relatively poor for low levers of molecular targets and suffers from a lack of cell specificity compared to other imaging modalities. Therefore, nanoparticles-based multimodal imaging probes have been developed for more accurate imaging and diagnosis.¹⁰⁻¹³ On the other hand, optical imaging has excellent sensitivity at subcellular levels and for quantifying molecular events, but its limited capability in examining deep tissue restricts collection of information in vivo. Therefore, a single nanoprobe, useful for both MR and optical imaging, would lead to novel tools for research and life science due to the highly complementary capabilities of the two imaging technologies. The use of a single probes with both imaging technology minimizes artifacts and enables significant improvement in diagnostic accuracy and therapeutic strategy, in comparison with standalone imaging.¹⁴

In searching for new imaging agents integrated with different modalities, quantum dots have drawn much attention as a convenient scaffold. Nanoparticles have several advantages over conventional molecular fluorophores.¹⁵ Their emission wavelength can be tuned by varying their size and composition and, due to their narrow emission width, it is easier to perform multicolor imaging with minimal spectral overlap. Due to their broad excitation spectra, it is possible to excite all colors of quantum dots simultaneously with a single light source.¹⁶ Furthermore, they display excellent photostability over molecular fluorophores. These unique optical properties have allowed quantum dots to emerge as a strong competitor as fluorescent probes for labeling experiments.¹⁷⁻¹⁹ Thus, the integration of T₁-weight MR imaging agents with quantum dots would be highly

desirable. Recently, MRI/optical nanoparticles have been designed that involve attachment of Gd^{3+} chelates to CdSeTe/CdS,²⁰ CdSe,²¹⁻²³ CdTe/ZnS quantum dots.²⁴ However, their widespread biological use is severely limited by the presence of cadmium as a major component in most commercially available quantum dots. A number of reports discussed the toxicity effects of cadmium-based quantum dots, as cadmium ions may diffuse into the biological environment with time.²⁵ In addition to possible effects on health, there are significant environment concerns regarding the use and disposal of cadmium-based nanomaterials. This has motivated the search for alternative semiconducting materials that are not only technologically useful but also environmentally benign. I-III-VI ternary nanoparticles, such as CuInS₂-based nanomaterials, are emerging as one such promising candidate. They do not contain toxic elements and, being direct band-gap semiconductors, their optical properties can be tuned by composition and size.

Mesoporous silica nanoparticles received considerable attention in the past few decades due to their stability, biocompatibility, versatile surface chemistry and precisely defined nanoporosity.²⁶⁻²⁸ It has been pointed that two approaches—stober sol-gel chemistry and microemulsion—can be used to encapsulate quantum dots with silica.^{29,30} Interestingly, Hyeon *et al.* developed a new method to coat magnetic nanoparticles with mesoporous silica.³¹ Compared to the traditional stober sol-gel chemistry and microemulsion methods, the Hyeon methods is simple and the thickness of the silica shell is tunable. Gao and coworkers have succeeded in exploiting this method to prepare and mesoporous silica-coated quantum dots.³²

Herein, we report a new MR/optical nanoparticles based on silica-coated CuInS₂/ZnS with covalent attachment of a Gd^{3+} -complex. In brief, the as-prepared CuInS₂/ZnS nanoparticles were transferred into water with the assistance of cetyltrimethylammonium bromide (CTAB) first. Tetraethylorthosilicate (TEOS), as the silica source, was then added and its hydrolysis led to the growth of silica shell onto the CuInS₂/ZnS nanoparticles. The silica-coated nanoparticles were aminated through silanization, which enabled further conjugation of Gd^{3+} -DTPA (diethylenetriaminepentaacetic acid) complex on their surface. To assess the effectiveness of the proposed dual-modality nanoparticles as an MRI contrast agent, the magnetic resonance relaxivity of the dual-modality nanoparticles was measured using a clinical MR scanner at room temperature. The cellular imaging of the nanoparticles was also successfully demonstrated by using human pancreatic cancer cell lines BXP-3 cells.

2. Experimental

2.1. Materials

Cu(I) iodide (CuI, 99.998%), In(III) acetate (In(OAc)₃, 99.99%), 1-octadecene (ODE, 90%), $Gd(NO_3)_3 \cdot 6H_2O$ were purchased from Alfa Aesar. All other chemicals were purchased from Shanghai Chemical Reagent Co. All chemicals were used without further purification.

2.2. Synthesis of CuInS₂ core and CuInS₂/ZnS core/shell nanoparticles

The synthesis CuInS₂ with different Cu/In compositions of 1/1,

1/2, 1/4 were prepared by fixing the amount of In precursor and varying the amount of Cu precursor. For a typical synthesis of CuInS₂ with a Cu/In 1/1, CuI (0.4 mmol) and In(Ac)₃ (0.4 mmol) were mixed with 1 mL of DDT and 8 mL of ODE in a 50 mL three-neck flask under an inert atmosphere.³⁵ The mixture was heated to 80°C under a vacuum and magnetic stirring for 1 h, backfilled with N₂, and heated to the reaction temperature of 230°C within 10 min. The growth of CuInS₂ core was allowed for 10 min at that temperature. CuInS₂ with Cu/In ratios of 1/2, 1/4 were synthesis in exactly the same way as above except using 0.2 and 0.1 mmol of CuI, respectively. For the ZnS shell overcoating, the ZnS precursor solution was prepared by dissolving 3.2 mmol of zinc stearate in 5 mL of ODE. The shell precursor solution was added dropwise at a rate of 1.0 mL/min into the CuInS₂ core crude solution at 230°C. The mixture maintained at that temperature for optimum shell overcoating times of 30-40 min. As-reacted CuInS₂ core and CuInS₂/ZnS core/shell nanoparticles were precipitated with an excess of ethanol, purified repeatedly with a solvent combination of chloroform/ethanol by a centrifugation, and finally dispersed in chloroform.

2.3. Synthesis of CuInS₂/ZnS@SiO₂ nanoparticles

The silica coating process was adopted from the published papers with some modifications.^{33,34} Typically, 1 mL solution of chloroform containing 10 mg of CuInS₂/ZnS nanoparticles was added to 5 mL 0.25 M cetyltrimethylammonium bromide (CTAB) solution. After vigorous vortex and sonification for 40 min, the opaque solution became semitransparent gel. The gel was then heated to 70°C to evaporate the chloroform, leaving a transparent red brownish solution. The formed solution was added to a mixture of 45 mL of water and 0.3 mL of 2 M NaOH solution. The mixture was then heated 70°C. Subsequently, TEOS and ethylacetate were dropped into the reaction solution. The reaction was kept on stirring for 3 h and allowed to slowly cool down to room temperature. The silica encapsulated quantum dots were rinsed with ethanol repeatedly to remove the unreacted precursors.

2.4. Functionalization of CuInS₂/ZnS@SiO₂ nanoparticles

To conjugate CuInS₂/ZnS@SiO₂ nanoparticles with Gd-DTPA, the bare silica surface was pre-modified with APS. Approximately 2 mg of CuInS₂/ZnS@SiO₂ nanoparticles were dissolved in 10 mL ethanol and 10 μ L APS was then added. The mixture was allowed to keep stirring overnight and the aminated particles were collected by centrifugation. These nanoparticles were washed with ethanol several times and then suspended in ethanol again. For further functionalization of the surface amine groups of the CuInS₂/ZnS@SiO₂-NH₂ nanoparticles with diethylenetriaminepentaacetic acid (DTPA) moieties, the CuInS₂/ZnS@SiO₂-NH₂ were dispersed into dry DMF. Then, triethylamine (0.36 mL) and diethylenetriaminepentaacetic acid dianhydride (DTPAda) (72 mg) was added to the nanoparticle suspension. The mixture was heated to 80°C for 30 min, and cooled down to room temperature while stirring overnight. The nanoparticles were purified by repeating the centrifugation/redispersion/washing steps: 2 times with 1% triethylamine in DMF, 2 times with water, and 2 times with acetone, followed by drying in vacuum before use. By varying the concentration of DTPAda, CuInS₂/ZnS@SiO₂(DTPA)-NH₂

nanoparticles were obtained. The DTPA-functionalized nanoparticles were stored at 4°C before use.

2.5. Loading Gd³⁺ ions to DTPA-functionalized nanoparticles

In a typical process, the prepared CuInS₂/ZnS@SiO₂(DTPA)-NH₂ nanoparticles (20 mg) were dispersed in Tri-HCl buffer solution (pH=7.4, 10 mL, 0.05M). Then, a Gd(NO₃)₃ · 6H₂O aqueous solution (1 mL, 10 mM), were added dropwise into the nanoparticles suspension while stirring. After 12 h, the nanoparticles were centrifuged and redispersed in water for at least three times. The obtained Gd³⁺-loaded CuInS₂/ZnS@SiO₂(DTPA)-NH₂ nanoparticles were finally dispersed in water to form a pale white transparent solution.

2.6. Cytotoxicity testing and in vitro microscopy imaging.

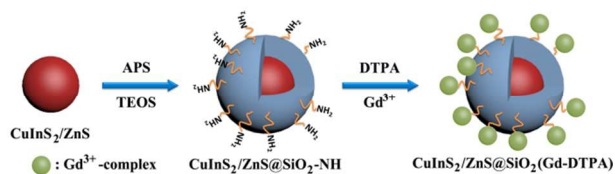
A cell counting Kit-8 assay kit (Beyotime, China) was employed to evaluate the toxicity of the samples. Briefly, the cells were seeded into a 96-well plate (Corning, USA) and grown to a density of 10⁴ cells per well. Then serial dilutions of the samples were added and incubated with the cells for 24 h. Subsequently, CCK-8 solution (20 μL per well) was added and the plate was further incubated for 30 min. The absorbance of each well at 450 nm was finally measured with a microplate reader (Infinite M200, Tecan).

Human pancreatic cancer cell lines BXPC-3 cells were placed in a 96-well plate, and grown at 37°C and 5% CO₂ in air. After seeding 24 h, 100 μL of nanoparticles with the concentration of 10 μg mL⁻¹ were added to each well. After incubation for 3 h, the cells were observed using an Olympus Fluoview 300 confocal laser scanning system with 488 nm argon laser excitation.

2.7. Characterization

UV-vis and PL spectra were obtained on a Shimadzu UV-2450 UV-vis spectrophotometer and a Cary Eclipse (Varian) fluorescence spectrophotometer, respectively. The room temperature QYs of nanoparticles were determined by comparing the integrated emission of nanoparticles in solution with that of rhodamine B in ethanol solution. The known QYs of the nanoparticles in solution can be used to measure the PL efficiencies of other nanoparticles by comparing their integrated emission. To conduct an investigation by TEM, the nanoparticles were deposited from dilute toluene solutions onto copper grids with carbon support by slowly evaporating the solvent in air at room temperature. TEM images were acquired using a JEOL JEM-2100 transmission electron microscope operating at an acceleration voltage of 120 kV. Elemental compositions of quantum dots were determined by energy-dispersive X-ray spectroscopy (EDX, Fison 60s, EDAX, USA) and X-ray photoelectron spectroscopy (XPS, PHI5000 VersaProbe, ULVAC-PHI Inc., Japan). XRD was obtained by wide-angle x-ray scattering using a Siemens D5005 X-ray powder diffractometer equipped with graphite-monochromatized Cu Kα radiation (λ=1.54178 Å). XRD samples were prepared by depositing nanoparticles on a piece of Si(100) wafer. ICP-AES (Optima 7300DV, Perkin-Elmer) was used to measure the concentrations of Gd elements in the samples. MRI was obtained by NMR relaxivity. MRI imaging experiments were performed at room temperature on a Biospec 3T system equipped with the standard gradient set. The longitudinal (r₁) relaxivity was determined as the slope of the line for plots of 1/T₁

against increasing manganese concentration with a correlation coefficient greater than 0.99.



Scheme 1. Synthetic route for generation of CuInS₂/ZnS@SiO₂(Gd³⁺-DTPA) nanoparticles.

3. Results and discussion

CuInS₂/ZnS nanoparticles were prepared following the previous protocols by using 1-dodecanethiol (DDT), containing long hydrocarbon tails as a hydrophobic protective agent and ODE as solvent.³⁵ ODE is a low-cost, low-hazard, and air-stable liquid at room temperature, which boils at about 320°C. During heat treatment, monomers accumulate in the ODE solution and burst nucleation occurs to generate seeds above the critical concentration. To improve the PL efficiency, ZnS materials, having a wide direct bandgap to confine both electrons and holes in the core, was used as an inorganic shell for surface passivation of the CuInS₂ nanoparticles. XRD patterns of three CuInS₂ core with Cu/In molar ratios of 1/1, 1/2, 1/4 in the starting solution concentration were compared in Figure 1, where no distinguishable difference in reflection peak angle was observed despite a relatively large variation of Cu content in CuInS₂. Three distinct reflection peaks with 2θ values of 28.0°, 46.5°, 54.9° could be well indexed to (112), (204)/(220), and (116)/(312) planes of a known tetragonal chalcopyrite structure of the CuInS₂ core.³⁶ The XRD results were consistent with those published in the literature, where the XRD pattern of highly off-stoichiometric (Cu/In ratio of 1/7) CuInS₂ was the same as that of stoichiometric ones (Cu/In ratio of 1/1).³⁷ A certain metastable, In-rich CuInS₂ phase such as CuIn₃S₅ might be expected to be generated under the Cu-deficient synthesis; however, the identification of such a metastable phase is practically challenging due to its structural similarity to the CuInS₂ phase and XRD peak broadening. Nevertheless, based on Raman spectroscopic results on CuInS₂ with various degrees of Cu deficiency analyzed by Uehara et al.,³⁷ our off-stoichiometric CuInS₂ with Cu/In ratios of 1/2, 1/4 are thought to possess the same chalcopyrite framework as stoichiometric nanoparticles, although such Cu-deficient nanoparticles are likely to include a high density of Cu-deficient nanoparticles (e.g., Cu vacancy and In interstitial at the Cu site). Overcoating of the ZnS shell was conducted under an identical condition for the above three CuInS₂ core. XRD patterns of all core/shell nanoparticles after ZnS shelling were also the same (Figure 1), as expected. Since the lattice parameter (a = 0.5517 nm) of chalcopyrite CuInS₂ is larger than that (a = 0.5345 nm) of zinc blende ZnS, the reflection peaks of CuInS₂/ZnS nanoparticles shifted to a larger 2θ compared to CuInS₂ core ones, closely approaching those of (111), (220), and (311) planes of the zinc blende ZnS phase and thus indicating that the ZnS overlayer was deposited appropriately on the surface of respective CuInS₂ core. TEM work on CuInS₂ with different Cu/In ratios was conducted, but the difference in shape and size was not observed

between those CuInS_2 . Figure 2a presents a TEM image of representative CuInS_2 with a $\text{Cu/In} = 1/1$, whose size was widely dispersed in the range of 2.5-3.0 nm. Such a size distribution is usually inherent in the noninjection-based synthetic route and can be partially attributed to a continual release of the S ion from the DDT molecule throughout the reaction. Upon ZnS shelling on the same CuInS_2 ($\text{Cu/In} = 1/1$), the overall size of core/shell nanoparticles increased to 4.0-4.5 nm, as seen from Figure 2b. Similar to the size distribution of CuInS_2 , that of $\text{CuInS}_2/\text{ZnS}$ nanoparticles was also wide, conjecturing that the thickness of the ZnS shell deposited on different-size CuInS_2 might be roughly the same. Figure 3c displays the TEM image of the aminated $\text{CuInS}_2/\text{ZnS}@/\text{SiO}_2\text{-NH}_2$ nanoparticles. Calculated from the observation of the TEM image, the average diameter of the $\text{CuInS}_2/\text{ZnS}@/\text{SiO}_2\text{-NH}_2$ nanoparticles was around 30 nm. However, CTAB molecules are toxic to the cultivated cells. For further biological applications, therefore, the CTAB was removed by repeatedly washing the nanoparticles with ethanol and water to diminish their cell toxicity. For conjugation of Gd^{3+} complex onto the surface of $\text{CuInS}_2/\text{ZnS}@/\text{SiO}_2\text{-NH}_2$ nanoparticles, diethylenetriaminepentaacetic acid (DTPA) was reacted with the primary amine group of $\text{CuInS}_2/\text{ZnS}@/\text{SiO}_2\text{-NH}_2$ nanoparticles through the formation to amide bonds.³⁷ To complex Gd ions via a strong chelation bond with carboxyl groups of DTPA, the DTPA-conjugated $\text{CuInS}_2/\text{ZnS}@/\text{SiO}_2\text{-NH}_2$ nanoparticles were mixed with an excess amount of $\text{Gd}(\text{NO}_3)_3 \cdot 6\text{H}_2\text{O}$. Free Gd^{3+} ions were removed by dialysis. Figure 2d show the $\text{CuInS}_2/\text{ZnS}@/\text{SiO}_2(\text{Gd-DTPA})\text{-NH}_2$ nanoparticles after complete functionalization. The mean diameter of the nanoparticles was increased to 34 nm.

The chemical compositions of three CuInS_2 core were assessed by EDS measurements, and their compositional spectra and quantitative results are Figure 3a. Actual Cu/In composition ratios of CuInS_2 with $\text{Cu/In} = 1/1, 1/2, 1/4$ were calculated to be 1.00, 0.49, and 0.25, respectively, which were almost identical with the solution mole ratios used for CuInS_2 synthesis. For all CuInS_2 samples, a somewhat excess content of S was detected; for instance, Cu:In:S was measured to be 0.486:1:2.32 in the case of CuInS_2 with $\text{Cu/In} = 1/2$, being ascribed to the contribution of S from the cation capping surface ligand of DDT. As seen from the EDS spectra of all $\text{CuInS}_2/\text{ZnS}$ nanoparticles samples in Figure 3b, the signals of Cu and In lines were significantly attenuated after ZnS shelling by the predominance of Zn peaks, and in particular, the $\text{Cu } L_{\alpha}$ line appeared to buried in the $\text{Zn } L_{\alpha}$ line due to a close proximity in energy. Compared to bare CuInS_2 , the Cu/In ratios of $\text{CuInS}_2/\text{ZnS}$ nanoparticles were almost maintained. Assuming that the cation (Cu and In) precursors added for CuInS_2 synthesis were almost consumed and considering that the Zn/In ratio in the starting solution concentration for all CuInS_2 was 8, a relatively low actual Zn content resulted for all $\text{CuInS}_2/\text{ZnS}$ nanoparticles. This observation indicates that all Zn stearate added for shell overcoating did not participate in the formation of ZnS overlayer, and the remaining precursor would stay as an unreacted part and/or generate byproducts, both of which were ultimately washed out during purification processing. XPS provided further evidence for the growth of the ZnS shell on the CuInS_2 core with $\text{Cu/In} = 1/1$, as shown in Figure S1. In agreement with the EDX

measurements, XPS detected the peak centered around 1021 and 1024 eV for Zn 2p. Moreover, the valence states of In^{3+} , Cu^+ and S were also confirmed by XPS spectra.

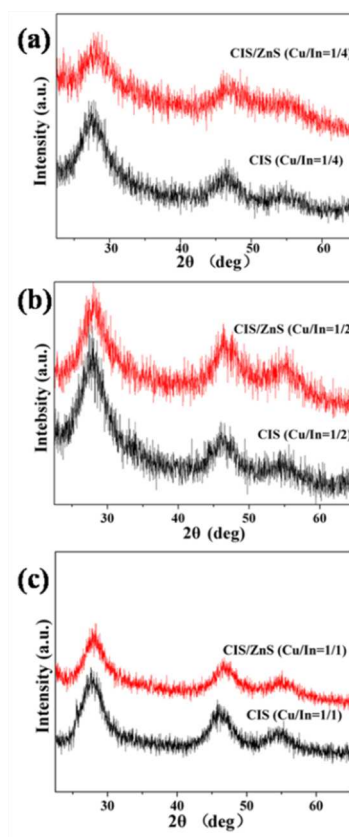


Figure 1. XRD patterns of CuInS_2 and $\text{CuInS}_2/\text{ZnS}$ nanoparticles synthesized by using Cu/In ratios of 1/4 (a), 1/2 (b), 1/1 (c).

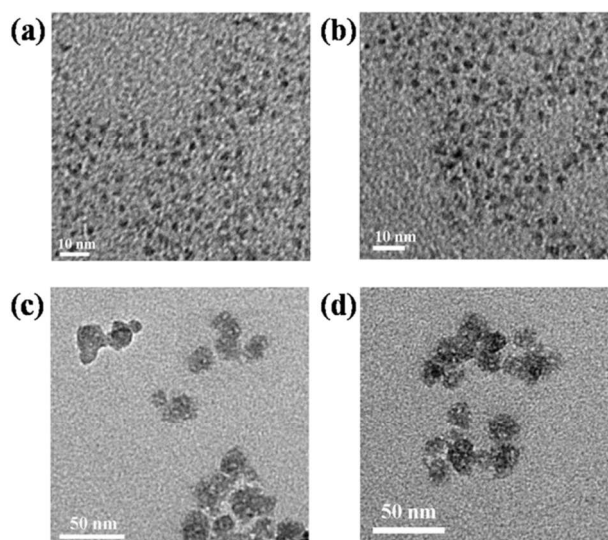


Figure 2. TEM micrographs of nanoparticles from typical synthesis showing diameters of (a) 2.5 nm for CuInS_2 , and (b) 4 nm for core/shell $\text{CuInS}_2/\text{ZnS}$ nanoparticles. (c) TEM micrographs of $\text{CuInS}_2/\text{ZnS}@/\text{SiO}_2\text{-NH}_2$ nanoparticles. (d) TEM micrographs of $\text{CuInS}_2/\text{ZnS}@/\text{SiO}_2(\text{Gd-DTPA})\text{-NH}_2$ nanoparticles.

Figure 4a presents absorption spectra of CuInS_2 with different

Cu/In ratios, where a blueshift in absorption from more Cu-deficient CuInS₂ is evident. This blueshift is not related with size variation. Such a variation of the Cu/In composition-dependent band gap in CuInS₂ is consistent with the previous reports, where this phenomenon is generally attributable to the lowering of valence band due to the weakened repulsion between Cu d and S p orbitals in Cu-deficient material, ultimately leading to a band gap widening.^{38,39} As seen from the normalized emission spectra in Figure 4b, all core emitted in the deep red region (with peak wavelengths of 711 nm for Cu/In = 1/1 and 654 nm for Cu/In = 1/4) with broad emission bandwidths of 121-130 nm. A systematic blueshift of emission observed from the sample with a higher degree of Cu deficiency should be associated with a band gap widening as described above. Large Stokes shifts of emission versus absorption wavelength up to ~650 meV imply that the radiative decay should not stem from the carrier recombination between quantized electron-hole levels but be involved with internal and / or surface defects sites that serve as intragap states, although the accurate assignment of electron-hole recombination channels in CuInS₂ still seems ambiguous. The broad bandwidth of emission is characteristic of defect-related radiative transition like the case of CuInS₂. The nanoparticles size inhomogeneity might lead to a broadened feature of emission. However, a recent report suggested that through the comparison of size-selective precipitated CuInS₂ an improvement of size inhomogeneity rarely modified the emission bandwidth,⁴⁰ reinforcing the above defect-related recombination mechanism. Emission QYs of CuInS₂ with Cu/In = 1/1, 1/2, 1/4 were measured to be 3.7, 6.4, 7.8%, respectively. Such an increasing trend in QY with more Cu-deficient nanoparticles coincide with the results reported from Uehara³⁷ and Nam et al.³⁸ A higher density of Cu-related defect states generated by intentionally preparing Cu-deficient nanoparticles would give rise to a higher probability of carrier recombination, resulting in an enhanced efficiency.

ZnS overcoating was conducted on CuInS₂ core with Cu/In ratios of 1/1, 1/2, and 1/4. As the band gap of the CuInS₂ core in CuInS₂/ZnS nanoparticles increase, emission spectra of all CuInS₂/ZnS nanoparticles were blue-shifted relative to their respective CuInS₂ core counterparts, showing 630 nm, 602 nm, and 562 nm emission from CuInS₂/ZnS nanoparticles with Cu/In = 1/1, 1/2, 1/4, respectively (Figure 4c), accompanying the dramatic rise in emission QY. Owing to the effective surface passivation by the ZnS overlayer, the QYs of CuInS₂/ZnS nanoparticles with Cu/In = 1/1, 1/2, 1/4 were enhanced to 51, 56, and 62%, respectively. It is worth noticing that the PL emission spectra of the corresponding CuInS₂/ZnS@SiO₂ nanoparticles demonstrated red shift unexceptionally (Figure 4d). The emission wavelengths of the CuInS₂/ZnS@SiO₂ nanoparticles with Cu/In = 1/1, 1/2, 1/4 were determined at 647 nm, 620 nm, and 598 nm by a luminescence spectrometer, respectively. The PL emission red shifts of silica coated CdSe and CdTe synthesized by the reverse microemulsion method were reported by other researchers previously. Although the mechanism remains unclear, this change in PL spectra is usually attributed to the ligand replacement and change in surface charge.⁴¹ It is well known that surfactants play an important role in surface passivation by forming bonds with exposed atoms on the surface and protecting surface defects. Therefore the change in the surface state greatly affects the

photophysical properties of quantum dots. Besides, several investigations have proven that charges, especially negative charges, in the vicinity of quantum dots can generate an electric field which is sufficient to influence the radiative recombination rate of electron-hole pairs.⁴¹ Subsequently, the emission spectra of quantum dots can be quenched and red-shifted. As for the case of CuInS₂/ZnS@SiO₂ nanoparticles in this study, the primary surfactant n-DDT with -SH can bind to the Zn atoms strongly. Thus the ligand exchange is less likely to be the possibility. Therefore, the surface charges, such as hydroxyl ions and Si-O⁻ that are accompanied with the silica shell, might be considered as the major cause of the red shift. Besides, the overall size of the CuInS₂/ZnS@SiO₂ nanoparticles was increased due to the silica coating, which might contribute to the red shift of the emission too.

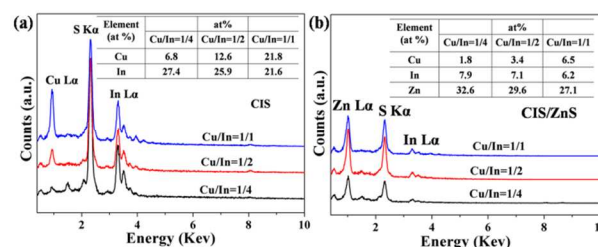


Figure 3. EDS spectra and calculated atomic ratio (insets) of (a) CuInS₂ and (b) CuInS₂/ZnS nanoparticles synthesized under different Cu/In ratios of 1/1, 1/2, 1/4.

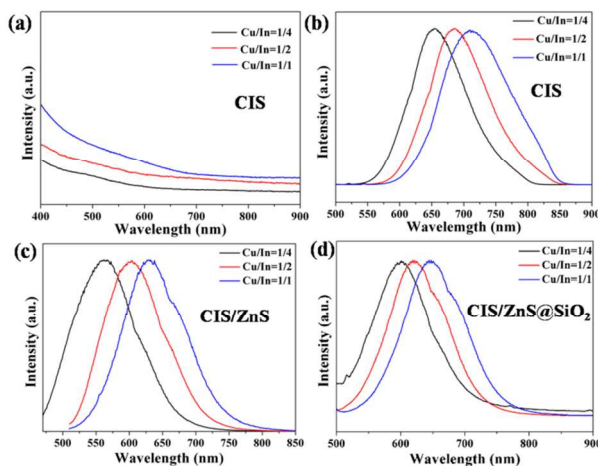


Figure 4. (a) Absorption and normalized (b) PL emission spectra of CuInS₂ synthesized under different Cu/In ratios of 1/1, 1/2, 1/4. PL emission spectra of CuInS₂/ZnS nanoparticles (c); and CuInS₂/ZnS@SiO₂-NH₂ (d) synthesized under different Cu/In ratios of 1/1, 1/2, 1/4.

The MR imaging mechanisms are based on excitation and relaxation of hydrogen nuclei that are abundant in water and lipids of tissue. The intrinsic longitudinal (T_1) and transverse (T_2) relaxation times of different parts of biological tissue bring about changes in MR signal intensity, which in turn results in an imaging contrast. To validate the potential of the nanoparticles as a contrast agent, we acquired the T_1 -weighted MR images and measured the relaxation rates as a function of metal concentration using a 3.0 T MRI scanner. As shown in Figure 5, the nanoparticle (Figure 5b) induced a bright signal enhancement in a

concentration-dependent manner on the T_1 -weighted images. It should be noted that they exhibited better T_1 positive contrast compared to a clinically available Gd-DTPA-based contrast agent (Magnevist, Figure 5a). Moreover, the specific relaxivity (r_1) of the nanoparticles ($8.45 \text{ mM}^{-1}\text{s}^{-1}$) was markedly higher than r_1 of Magnevist ($5.4 \text{ mM}^{-1}\text{s}^{-1}$), suggesting that they were much more efficient in enhancing T_1 positive contrast than Magnevist. It was reported previously that the r_1 values of Gd-based contrast agents were strengthened when bound to large molecules such as proteins and polymers due to the limited molecular motion of Gd^{3+} ions.⁴² Hence, it was conceivable that the remarkably high r_1 value of the nanoparticles resulted from the reduced mobility of Gd^{3+} ions tightly incorporated into nanometer-scale particles. Since the covalently immobilized DTPA shell on the nanoparticles allowed for strong coordination of Gd^{3+} ions onto the particles, the nanoparticles were considered to be safer than aqueous $\text{Gd}(\text{NO}_3)_3$ solution.

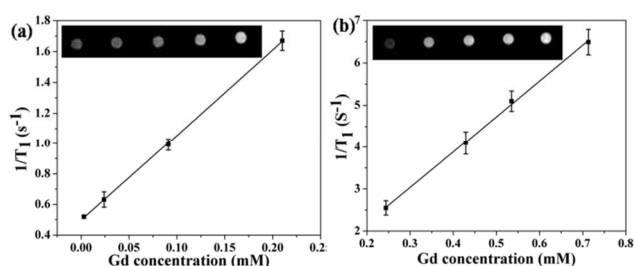


Figure 5. T_1 -weighted magnetic resonance images of (a) Gd-DTPA, (b) $\text{CuInS}_2/\text{ZnS}@\text{SiO}_2(\text{Gd-DTPA})-\text{NH}_2$.

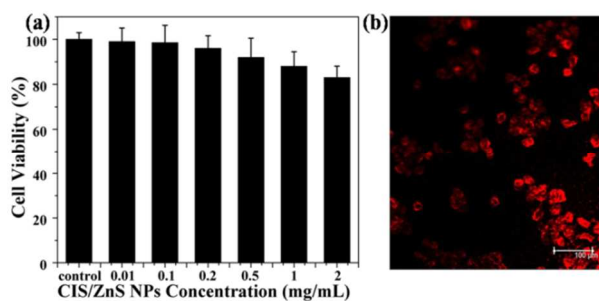


Figure 6. (a) Cytotoxicity evaluation of the nanoparticles in the BXPC-3 cells. (b) Fluorescent image of BXPC-3 cells tagged with the nanoparticles with red emission under 488 nm argon laser excitation. Scale bar = 100 μm .

Before optical imaging, we briefly assessed the cytotoxicity of the nanoparticles by using standard MTT assay (Figure 6a). The results showed that cytotoxicity of the nanoparticles is low due to many factors, including the use of the elements with low toxicity. To determine the potential of using these nanoparticles with high relaxivity and photoluminescence as multimodal probes for in vitro fluorescence imaging in living cells. We incubated human pancreatic cancer cell lines BXPC-3 cells with the nanoparticles for 3 h and then observed the cells with confocal microscopy. As shown in Figure 6b, it is clear that the BXPC-3 cells tagged with the nanoparticles emitted clear red emission under 488nm argon laser excitation, indicating that the nanoparticles were readily internalized into human pancreatic cancer cells lines BXPC-3 cells. Then, the cells were lysed and imaged by MRI as shown Figure 7. Cells that were incubated

with the nanoparticles show significant contrast enhancement from unlabeled cells in a T_1 -weighted image. It is demonstrated that the same range of applied concentration can produce contrast for optical and MR imaging and illustrate the dual-mode utility of the nanoparticles would provide a novel candidate for cell imaging and biomedical research in the further.



Figure 7. Internalized quantum dots produce MRI contrast. T_1 -weighted images from tubes containing cell lysates show that lysates of cells that have been incubated with quantum dots (right) show significant contrast enhancement as compared to cells that have not been exposed to quantum dots. The samples were from cells in the same experiment shown for the optical uptake studies of Figures of 6.

4. Conclusions

Herein, we demonstrate the facile fabrication of Gd-based $\text{CuInS}_2/\text{ZnS}$ nanoparticles with magnetic resonance/optical imaging capability. This dual-modality nanoparticles demonstrated good biocompatibility with respect to in vitro cytotoxicity tests conducted by MTT assay on BXPC-3 cells. MR imaging characterization revealed that the dual-modality nanoparticles elicits T_1 relaxivity ($r_1 = 8.45 \text{ mM}^{-1}\text{s}^{-1}$) and we can observe a clear, positive, and increasing contrast enhancement of magnetic resonance signals concurrently with an increasing Gd^{3+} concentration of nanoparticles. Confocal scanning laser imaging characterization revealed that the BXPC-3 cells can be tagged with the nanoparticles, which would be beneficial for evaluating the stage of tumor progression and making treatment decisions. These results indicate that the nanoparticles has potential to be used as platform for dual-modality imaging in various biological systems. We expect that these results will open up a way to take advantage of the full potential of I–III–VI quantum dots for biological in vitro and in vivo studies.

Acknowledgements

This work was supported by the National Natural Science Foundation of China (21236003, 21206042, 20925621, and 21176083), the Basic Research Program of Shanghai (13NM1400700, 13NM1400701), and the Fundamental Research Funds for the Central Universities.

References

- ^aKey Laboratory for Ultrafine Materials of Ministry of Education, School of Materials Science and Engineering, East China University of Science and Technology, Shanghai 200237, China. Fax: +86 21 6425 0624; Tel: +86 21 6425 2022; E-mail: yhzhu@ecust.edu.cn
- ^bDepartment of Radiology, Zhongshan Hospital of Fudan University and Department of Medical Image, Shanghai Medical College of Fudan University, Shanghai Institute of Medical Imaging, 138 Fenglin Road, Shanghai 200032, China.
- [†]These authors contributed equally to this work.
- [†]Electronic Supplementary Information (ESI) available: Detailed and additional Figures as noted in the text. See DOI: 10.1039/b000000x/
- N. Tran and T. J. Webster, *J. Mater. Chem.*, 2010, **20**, 8760.

- 2 Y. Zhang, G.S. Hong, Y.J. Zhang, G.C. Chen, F. Li, H.J. Dai and Q. B. Wang, *ACS Nano*, 2012, **6**, 3695.
- 3 A. Louie, *Chem. Rev.*, 2010, **110**, 3146.
- 4 Q. Chen, K. G. Li, S. H. Wen, H. Liu, C. Peng, H. D. Cai, M. W. Shen, G. X. Zhang and X. Y. Shi, *Biomaterials*, 2013, **34**, 5200.
- 5 B. Shah, P. T. Yin, S. Ghoshal and K. B. Lee, *Angew. Chem. Int. Ed.*, 2013, **52**, 6190
- 6 R. D. Corato, F. Gazeau, C. L. Visage, D. Fayol, P. Levitz, F. Lux, D. Letourneur, N. Luciani, O. Tillement and C. Wilhelm, *ACS Nano*, 2013, **7**, 7500.
- 10 7 W. Fan, B. Shen, W. B. Bu, F. Chen, K. Zhao, S. J. Zhang, L. P. Zhou, W. J. Peng, Q. F. Xiao, H. Y. Xing, J. N. Liu, D. L. Ni, Q. J. He and J. L. Shi, *J. Am. Chem. Soc.*, 2013, **135**, 6494.
- 8 M. F. Kircher, A. Zeral, J. V. Jokerst, C. L. Zavaleta, P. L. Kempen, E. Mittra, K. Pitter, R. Huang, C. Campos, F. Habte, R. Sinclair, C. W. Brennan, I. K. Mellinghoff, E. C. Holland and S. S. Gambhir, *Nat. Med.* 2012, **18**, 829.
- 9 P. Caravan, *Chem. Sov. Rev.*, 2006, **35**, 512.
- 10 Y. S. Jin, J. R. Wang, H. T. Ke, S. M. Wang, *Biomaterials*, 2013, **34**, 4794.
- 20 11 S. J. Zeng, M. K. Tsang, C. F. Chan, K. L. Wong and J. H. Hao, *Biomaterials*, 2012, **33**, 9232.
- 12 J. Liu, W. Zhang, H. L. Zhang, Z. Y. Yang, T. R. Li, B. D. Wang, X. Huo, R. Wang and H. T. Chen, *Chem. Commun.*, 2013, **49**, 4938.
- 25 13 N. Lee, H. Kim, S. H. Choi, M. Park, D. Kim, H. C. Kim, Y. Choi, S. M. Lin, B. H. Kim, H. S. Jung, H. Kim, K. S. Park, W. K. Moon and T. Hyeon, *Proc. Natl. Acad. Sci. U. S. A.*, 2011, **108**, 2662.
- 14 W. J. Dong, Y. S. Li, D. C. Niu, Z. Ma, X. H. Liu, J. L. Gu, W. R. Zhao, Y. Y. Zheng and J. L. Shi, *Small*, 2013, **9**, 2500.
- 30 15 P. Subramaniam, S. J. Lee, S. Shah, S. Patel, V. Starovoytov and K. B. Lee, *Adv. Mater.*, 2012, **24**, 4014.
- 16 S. Sarkar, N. S. Karan and N. Pradhan, *Angew. Chem. Int. Ed.*, 2011, **50**, 6065.
- 17 G. S. Hong, J. T. Robinson, Y. J. Zhang, S. Diao, A. L. Antaris, Q. B. Wang and H. J. Dai, *Angew. Chem. Int. Ed.*, 2012, **51**, 9818.
- 35 18 I. Hocaoglu, M. N. Cizmeciyan, R. Erdem, C. Ozen, A. Kurt, A. Sennaroglu and H. Y. Acar, *J. Mater. Chem.*, 2012, **22**, 14674.
- 19 P. Jiang, C. N. Zhu, Z. L. Zhang, Z. Q. Tian and D. W. Pang, *Biomaterials*, 2012, **33**, 5130.
- 40 20 M. Oostendorp, K. Douma, M. T. Hackeng, J. M. Post, J. M. A. M. Zandvoort and H. W. Backes, *Magn. Reson. Med.*, 2010, **64**, 291.
- 21 R. Bakalova, Z. Zhelev, I. Aoki, K. Masamoto, M. Mileva, T. Obata, M. Higuchi, V. Gadjeva and I. Kanno, *Bioconjugate Chem.*, 2008, **19**, 1135.
- 45 22 P. Diagaradjane, A. Deorukhkar, G. J. Gelovani, M. D. Maru and S. Krishnan, *ACS Nano*, 2010, **4**, 4131.
- 23 J. Park, S. Bhuniya, H. Lee, Y. W. Noh, T. Y. Lim, H. J. Jung, S. K. Hong and S. J. Kim, *Chem. Commun.* 2012, **48**, 3218.
- 24 L. Liu, C. W. Law, T. K. Yong, I. Roy, H. Ding, F. Erogbogbo, X. Zhang, N. P. Prasad, *Analyst*, 2011, **136**, 1881.
- 50 25 A. M. Derfus, W. C. W. Chan and S. N. Bhatia, *Nano Lett.*, 2004, **4**, 11.
- 26 I. Slowing, B. G. Trewyn, S. Giri and V. S. Y. Lin, *Adv. Funct. Mater.*, 2007, **17**, 1225.
- 55 27 J. Pan, D. Wan and J. L. Gong, *Chem. Commun.*, 2011, **47**, 3442.
- 28 J. Nakazawa and T. D. P. Stack, *J. Am. Chem. Soc.*, 2008, **130**, 14360.
- 29 R. Bakalova, H. Ohba, Z. Zhelev, M. Ishikawa and Y. Baba, *Nat. Biotechnol.*, 2004, **22**, 1360
- 30 S. T. Selvan, P. K. Patra, C. Y. Ang and J. Y. Ying, *Angew. Chem. Int. Ed.*, 2007, **46**, 2448.
- 60 31 J. Kim, H. S. Kim, N. Lee, T. Kim, H. Yu, I. C. Song, W. K. Moon and T. Hyeon, *Angew. Chem. Int. Ed.*, 2008, **47**, 8438.
- 32 X. Hu, P. Zrazhevskiy and X. Gao, *Ann. Biomed. Eng.*, 2009, **37**, 1960.
- 65 33 J. Kim, H. S. Kim, N. Lee, T. Kim, H. Kim, T. Yu, I. C. Song, W. K. Moon and T. Hyeon, *Angew. Chem. Int. Ed.*, 2008, **47**, 8438
- 34 J. Kim, J. E. Lee, J. Lee, J. H. Yu, B. C. Kim, K. An, Y. Hwang, C. H. Shin, J. G. Park, J. Kim and T. Hyeon, *J. Am. Chem. Soc.*, 2006, **128**, 688.
- 70 35 L. Li, T. J. Daou, I. Texier, T. T. K. Chi, N. Q. Liem and P. Reiss, *Chem. Mater.*, 2009, **21**, 2422.
- 36 H. Zhong, S. S. Lo, T. Mirkovic, Y. Li, Y. Ding, Y. Li and G. D. Scholes, *ACS Nano*, 2010, **4**, 5253.
- 37 M. Uehara, K. Watanabe, Y. Tajiri, H. Nakamura and J. H. Maeda, *Chem. Phys.*, 2008, **129**, 134709.
- 75 38 E. D. Nam, S. W. Song and J. H. Yang, *J. Colloid Interface Sci.*, 2011, **361**, 491.
- 39 K. Y. Kim, H. S. Ahn, K. Chung, S. Y. Cho and J. C. Choi, *J. Mater. Chem.*, 2012, **22**, 1516.
- 80 40 R. Xie, M. Rutheerford and X. G. Peng, *J. Am. Chem. Soc.*, 2009, **131**, 5697.
- 41 S. A. Empeedocles and M. G. Bawendi, *Science*, 1997, **276**, 2114
- 42 M. F. Kircher, A. Zeral, J. V. Jokerst, C. L. Zavaleta, P. L. Kempen, E. Mittra, K. Pitter, R. Huang, C. Campos, F. Habte, R. Sinclair, C. W. Brennan, I. K. Mellinghoff, E. C. Holland and S. S. Gambhir, *Nat. Med.* 2012, **18**, 829.